H2O in nominally anhydrous mineral inclusions in diamonds and the volatile composition of diamond forming media

Andrea Curtolo, Maxwell C. Day, Francesca Innocenzi, Nathalie Bolfan-Casanova, Martha G. Pamato, Simon Falvard, Fabrizio Nestola, Jeff W. Harris, Davide Novella

Earth Planet. Sci. Lett. 658 (2025) 119311

Contents lists available at ScienceDirect

Earth and Planetary Science Letters

journal homepage: www.elsevier.com/locate/epsl

H_2O in nominally anhydrous mineral inclusions in diamonds and the volatile composition of diamond forming media

Andrea Curtolo [a,*], Maxwell C. Day [a], Francesca Innocenzi [a], Nathalie Bolfan-Casanova [b], Martha G. Pamato [a], Simon Falvard [b], Fabrizio Nestola [a], Jeff W. Harris [c], Davide Novella [a]

[a] Dipartimento di Geoscienze, Università degli Studi di Padova, Via Giovanni Gradenigo 6, Padova 35131, Italy
[b] Laboratoire Magmas et Volcans, CNRS-IRD-OPGC, Université Clermont Auvergne, 6 Avenue Blaise Pascal, Clermont-Ferrand 63170, France
[c] School of Geographical and Earth Sciences, University of Glasgow, Molema Building, Glasgow G12 8QQ, United Kingdom

ARTICLE INFO

Keywords:
Diamonds
Inclusions
H_2O
Cratons
FTIR
H diffusion

ABSTRACT

Many studies have investigated the H_2O content of mantle minerals in xenoliths, which in various cases show evidence of metasomatism, implying that the measured H_2O contents may reflect these modification processes rather than the H_2O content in the environment where they were sourced. In this work, the H_2O content of 118 mineral inclusions in lithospheric diamonds, that are shielded from metasomatic and alteration events by their diamond host, was investigated.

Most of the inclusions studied here are clinopyroxene and garnet of eclogitic and peridotitic paragenesis and their H_2O content was determined by recording Fourier Transform Infrared (FTIR) spectra of each inclusion within their diamond host. Additional analyses conducted on seven inclusions that were extracted from their diamond host show good agreement with the analysis performed while still trapped inside the diamond, confirming the validity of the H_2O contents determined for the inclusions still trapped by their diamond host. The measured H_2O contents range from 0 to 550 ppm wt. with eclogitic inclusions showing a higher H_2O content with respect to their peridotitic counterparts. On average, clinopyroxene has the highest H_2O content compared to all other inclusion minerals (with average H_2O content of 110 ppm wt. and 61 ppm wt. for eclogitic and peridotitic samples, respectively). The H_2O contents of mineral inclusions in diamonds studied here and from the literature are much lower than those reported for cratonic mantle xenoliths. This difference may be due to (i) sampling bias, (ii) metasomatism subsequent to diamond formation, or (iii) lithospheric mantle involved in diamond formation not being representative of the average cratonic lithosphere (i.e., with a different H_2O activity). Modelled H diffusion in mineral inclusions in diamonds at the pressure and temperature conditions of diamond formation is fast, indicating complete H_2O re-equilibration with the diamond forming medium. It follows that the diamond forming medium must be a silicate melt with a low H_2O content, a carbonatitic melt and/or a fluid characterized by a low H_2O activity.

1. Introduction

Studies on mantle rocks have shown that considerable amounts of H_2O are present in the cratonic lithosphere (see e.g., Demouchy and Bolfan-Casanova, 2016; Novella et al., 2024, and references therein) as H atoms bound to oxygens in the structure of nominally anhydrous minerals (NAMs). Even if present in trace concentrations (ppm wt.), H_2O has critical effects on the properties of the mantle such as its melting temperature (Green, 1973) and rheology (Hirth and Kohlstedt, 2003; Peslier et al., 2010), and in turn, controls the mantle compositional evolution and the stability of the lithosphere. Given the critical role played by H_2O in different geochemical and geodynamic processes, furthering our understanding of the distribution and behavior of H_2O (and volatiles in general) in the mantle remains imperative.

For these reasons, over the last 40 years, there has been an enormous amount of work (see e.g., Aines and Rossman, 1984; Moine et al., 2020; Aulbach et al., 2024) focused on investigating the H_2O content of NAMs from both cratonic and non-cratonic contexts (Skogby et al., 1990; Bell and Rossman, 1992a) to constrain where and how H_2O is stored in the mantle. These studies showed that NAMs can host large amounts of H_2O,

* Corresponding author.
E-mail address: andrea.curtolo.2@phd.unipd.it (A. Curtolo).

https://doi.org/10.1016/j.epsl.2025.119311
Received 31 October 2024; Received in revised form 26 February 2025; Accepted 7 March 2025
Available online 27 March 2025

even in old, depleted cratonic lithospheric settings, with H_2O contents reaching hundreds ppm wt. in olivine (Matsyuk and Langer, 2004; Jackson and Gibson, 2023), orthopyroxene (Bell and Rossman, 1992b; Chin et al., 2021) and garnet (Ragozin et al., 2014; Aulbach et al., 2023), and up to a striking 5065 ppm wt. in clinopyroxene (Moine et al., 2020). Careful examination of the geochemical signature of mantle xenoliths shows that their H_2O content reflects different degrees of metasomatism (see Doucet et al., 2014) combined with potential H_2O loss during kimberlite eruption. Assessment of the H_2O content of the cratonic lithosphere based on analyses of minerals in mantle xenoliths might therefore prove problematic as such minerals may not preserve the H_2O content of the mantle. Nevertheless, important information regarding the H_2O content of the mantle can still be retrieved from these samples.

Recently, attention has shifted to inclusions in diamonds as an alternative method to investigate the H_2O content of the deep mantle. During their formation, diamonds can encapsulate fragments of the ambient mantle as mineral inclusions and subsequently transport such inclusions to the surface while protecting them from physical breakdown and/or chemical alteration. Moreover, diamonds, being a product of metasomatic events themselves, could also provide important information regarding metasomatic fluids or melts in the mantle (Weiss et al., 2022). Mineral inclusions in diamonds have been studied extensively over the past decades providing fundamental information regarding the composition, petrology and chemistry of the mantle (see e.g., Aulbach et al., 2022a; Curtolo et al., 2023; Day et al., 2023). However, to date, only 12 studies reporting the H_2O content of inclusions in diamonds have been published (Kurosawa et al., 1997; Matsyuk et al., 1998; Koch-Müller et al., 2003; Matsyuk and Langer, 2004; Matveev and Stachel, 2009; Pearson et al., 2014; Novella et al., 2015; Jean et al., 2016; Taylor et al., 2016; Palot et al., 2016; Bassoo and Befus, 2021; Vangu et al., 2023). Notably, most of these studies focus on olivine and minimal work has been done on other mineral inclusions especially of the eclogitic paragenesis. Except for a ringwoodite inclusion found in a super-deep diamond from Brazil containing 1.4 wt% H_2O (Pearson et al., 2014), inclusions in lithospheric diamonds have lower H_2O contents compared to their counterparts in xenoliths. Clinopyroxenes, both in peridotitic and eclogitic substrates, are particularly important minerals, as they can host large amounts of H_2O and thus may comprise an important reservoir of H_2O in the mantle (Skogby, 2006). However, the H_2O content of only three clinopyroxene inclusions in diamond have been determined so far (Taylor et al., 2016). Clearly, more work investigating the H_2O content of NAM inclusions in diamonds is needed to improve our understanding of the H_2O content of the Earth's interior.

In this study, the H_2O content of 118 mineral inclusions in diamonds was determined. The samples studied here constitute a larger dataset than that currently available in the literature (101 inclusions). We focus primarily on clinopyroxene and garnet inclusions of both the eclogitic and peridotitic paragenesis as such samples are underrepresented in the available literature. The H_2O content of inclusions was determined using Fourier Transform Infrared (FTIR) spectroscopy. Single crystal X-ray diffraction and Raman spectroscopy were conducted to identify each inclusion and characterize their structure and composition. In addition, X-ray computed tomography (CT) analyses were conducted to obtain accurate thicknesses of each inclusion (ensuring accurate H_2O quantification) and to confirm that no fractures around the inclusions were present that could have allowed for alteration of the inclusion. The measured H_2O contents are compared with analogous data from inclusions in diamonds and minerals in xenoliths from the literature to discuss the presence and origin of H_2O in cratonic lithospheric mantle and the nature of volatiles in the diamond forming fluid/melt.

2. Materials and methods

2.1. Samples

In total, 114 inclusions were studied from 75 diamonds and four garnet inclusions already extracted from their diamond hosts were investigated in this work (Table 1). Samples are from different cratonic areas including the Kaapvaal (46), Zimbabwe (8), Siberian (8), Tanzanian (4) and North Australian (4) cratons. Moreover, two diamonds were collected from an alluvial placer deposit in the Urals (Russia) and three diamonds are of unknown origin.

Diamonds in this study are mainly colorless octahedra and rounded dodecahedra, but some irregular crystals, aggregates and macles are present. A number of yellowish diamonds and one greenish diamond are also present in the sample suite, with two examples shown in Fig. 1.

The mineral inclusion suite comprises 48 clinopyroxenes, 61 garnets, six olivines, and three orthopyroxenes. The paragenesis of each diamond was defined by the identified mineral inclusion(s) (e.g., presence of olivine), the color of garnet inclusions (Stachel and Harris, 2008) and based on Raman and X-ray diffraction analysis of some clinopyroxene inclusions.

Seven diamonds were broken to extract their inclusions and to validate the H_2O quantifications performed by FTIR analyses of the inclusions measured through the diamond and after their release from the diamond. These seven inclusions should not be confused with the four garnets mentioned above, as those were already released from their diamond host.

2.2. Raman spectroscopy

Analyses were performed with a Witec alpha 300R confocal Raman micro-spectrometer at the Dipartimento di Geoscienze (Università degli Studi di Padova, Italy) using a laser wavelength of 532 nm and a nominal laser power of 5 to 20 mW. All the major upper mantle minerals (olivine, pyroxenes and garnet) hosted as inclusions in diamond were identified and representative spectra of these phases are reported in Fig. S1. Clinopyroxene inclusions were assigned a peridotitic (diopside) or eclogitic (omphacite) paragenesis based on the observation of specific features in the respective Raman spectra (Fig. S1). Diopside usually exhibits a ~1015 cm^{-1} band with higher intensity than the ~665 cm^{-1} band (Smith et al., 2022), but this is not always the case as the intensity of the ~1015 cm^{-1} band in diopside is related to the orientation of the crystal, and in specific orientations, the ~665 cm^{-1} band is more intense (Prencipe et al., 2012). This observation was combined with the presence of sharp, discrete bands between 300 and 400 cm^{-1} to identify diopside, since omphacites display broad, overlapping bands in this region (Smith et al., 2022). Clinopyroxene spectra showing a more intense band at ~1015 cm^{-1} and/or sharp bands in the 300–400 cm^{-1} region were classified as diopside, and consequently assigned a peridotitic paragenesis. Clinopyroxenes showing a more intense ~665 cm^{-1} band and broad overlapping bands in the 300–400 cm^{-1} region were classified as omphacite and assigned an eclogitic paragenesis. This approach will assign pyroxenitic clinopyroxenes (which are diopsides) to the peridotitic suite. However, this has minimal effect on our interpretation since pyroxenitic inclusions comprise 2.3 % of the global database (Stachel and Harris, 2008).

Analyses of the interface of 73 (out of 114) mineral inclusions within the diamonds revealed two broad overlapping bands around ~620–670 and ~760–830 cm^{-1} (representative spectrum reported in Fig. S1), regardless of the characteristics of the diamond, its paragenesis, or the identity of the mineral inclusion. These bands were first observed by Nimis et al. (2016) and were attributed to fluid rims that contain $Si(OH)_4$ monomers and $Si_2O(OH)_6$ dimers in an aqueous solution. Further work in the present study using X-Ray CT (Section 2.4), regardless of resolution, to try and identify and then determine the nature of any fluid, in all cases failed, indicating that these rims in the present diamond set are extremely thin with a thickness <1–2 μm.

2.3. Single crystal X-ray diffraction

When phase identification with Raman spectroscopy was not

Table 1
List of all the diamonds analyzed in this work along with their provenance and geochemical data obtained from FTIR spectra.

Sample	Craton	Mine	Paragenesis	N_{tot} (at. ppm)	%B	Type	T_N (1 byr)	T_N (2 byr)	T_N(3 byr)	H_{3107}(cm^{-1})
DIO_01	Siberian	Udachnaya	P	343	78	IaAB	1198	1180	1169	1.54
DIO_02	Siberian	Udachnaya	P	25	52	IaAB	1238	1219	1208	0.02
ECLO_2	Siberian	Udachnaya	E	775	41	IaAB	1136	1119	1109	3.51
Grt_E_2	Siberian	Udachnaya	E	875	73	IaAB	1166	1149	1139	8.52
Grt_E_3	Siberian	Udachnaya	E	638	65	IaAB	1165	1148	1138	1.15
Grt_E_4	Siberian	Udachnaya	E	922	67	IaAB	1158	1141	1131	1.70
Grt_P_3	Siberian	Udachnaya	P	193	53	IaAB	1184	1166	1155	0.72
Grt_P_4	Siberian	Udachnaya	P	113	13	IaAB	1146	1129	1120	0.42
KF2	Kaapvaal	Koffiefontein	P	0	NA	II	NA	NA	NA	0.16
KF4	Kaapvaal	Koffiefontein	P	56	40	IaAB	1202	1184	1173	0.23
PM2	Kaapvaal	Bultfontein	P	11	26	IaAB	1230	1211	1200	0.00
PM4	Kaapvaal	Bultfontein	P	65	29	IaAB	1186	1168	1157	0.36
PR4	Kaapvaal	Cullinan	E	155	16	IaAB	1145	1128	1118	0.85
PR5	Kaapvaal	Cullinan	P	76	40	IaAB	1194	1176	1166	1.05
V10_01	NA	NA	E	108	12	IaAB	1144	1128	1118	0.13
V10_02	NA	NA	E	907	32	IaAB	1123	1106	1097	1.53
V10_03	NA	NA	E	0	NA	II	NA	NA	NA	0.00
DBP1–1	Kaapvaal	De Beers Pool	P	73	38	IaAB	1193	1175	1164	0.01
DBP1–2	Kaapvaal	De Beers Pool	P	87	24	IaAB	1171	1153	1143	0.34
DBP2–1	Kaapvaal	De Beers Pool	E	>776	NA	IaAB	NA	NA	NA	2.83
Dut1	Kaapvaal	Dutoitspan	E	>849	NA	IaAB	NA	NA	NA	1.82
Wes1	Kaapvaal	Wesselton	P	>641	NA	IaAB	NA	NA	NA	0.11
FinB14	Kaapvaal	Finsch	E	>656	NA	IaAB	NA	NA	NA	0.04
FinB15–1	Kaapvaal	Finsch	E	100	37	IaAB	1184	1166	1156	0.47
FinB15–2	Kaapvaal	Finsch	E	>880	NA	IaAB	NA	NA	NA	9.64
FinB15P7	Kaapvaal	Finsch	E	813	79	IaAB	1178	1160	1150	5.31
FinB15P3	Kaapvaal	Finsch	E	812	80	IaAB	1179	1161	1151	1.25
KFB65P24	Kaapvaal	Koffiefontein	P	0	NA	II	NA	NA	NA	0.00
KFB65P25	Kaapvaal	Koffiefontein	E	174	6	IaA	1115	1099	1090	0.00
VeB126P4–1-1	Kaapvaal	Venetia	P	604	53	IaAB	1154	1137	1127	0.62
VeB126P4–1-3	Kaapvaal	Venetia	E	815	79	IaAB	1177	1159	1149	2.79
VeB126P4–2	Kaapvaal	Venetia	P	278	51	IaAB	1172	1155	1145	0.19
Pr210–1	Kaapvaal	Cullinan	E	241	83	IaAB	1216	1197	1186	1.49
Pr210–2	Kaapvaal	Cullinan	E	391	79	IaAB	1196	1178	1168	1.48
Pr210–3	Kaapvaal	Cullinan	P	187	82	IaAB	1222	1203	1193	1.17
Pr210–4	Kaapvaal	Cullinan	E	697	57	IaAB	1154	1137	1127	0.19
Pr210–5	Kaapvaal	Cullinan	E	132	64	IaAB	1206	1187	1177	0.40
Pr210–6	Kaapvaal	Cullinan	E	722	73	IaAB	1172	1155	1145	0.23
Pr210–8	Kaapvaal	Cullinan	E	114	68	IaAB	1215	1196	1185	0.98
Pr210–9	Kaapvaal	Cullinan	E	84	65	IaAB	1219	1200	1189	0.98
Pr210–10	Kaapvaal	Cullinan	E	444	54	IaAB	1163	1146	1136	0.46
Pr210–11	Kaapvaal	Cullinan	E	545	69	IaAB	1173	1156	1146	0.50
OrB18P40–1	Zimbabwe	Orapa	E	151	49	IaAB	1186	1168	1158	0.45
OrB18P40–2	Zimbabwe	Orapa	P	55	43	IaAB	1206	1187	1177	0.30
JwB33L6–2	Kaapvaal	Jwaneng	P	950	88	IaAB	1191	1173	1162	2.24
JwB33A-1	Kaapvaal	Jwaneng	E	95	52	IaAB	1201	1183	1172	1.07
JwB33A-2	Kaapvaal	Jwaneng	E	746	67	IaAB	1163	1146	1136	4.37
JwB33B-1	Kaapvaal	Jwaneng	E	103	34	IaAB	1180	1162	1151	1.84
JwB33B-2	Kaapvaal	Jwaneng	E	181	27	IaAB	1156	1139	1129	2.81
JwB34P	Kaapvaal	Jwaneng	E	30	92	IaB	1303	1282	1270	0.34
LB18P68–1	Zimbabwe	Letlhakane	E	174	33	IaAB	1165	1148	1138	0.30
LB18P68–2	Zimbabwe	Letlhakane	E	33	42	IaAB	1220	1201	1190	0.61
Mw-1	Tanzanian	Mwadui	E	398	27	IaAB	1136	1120	1110	2.14
Mw-4	Tanzanian	Mwadui	E	443	85	IaAB	1204	1186	1175	2.10
UrP26	NA	Urals	E	482	85	IaAB	1202	1184	1173	1.26
UrP43	NA	Urals	E	471	70	IaAB	1179	1161	1151	1.41
ArB58T3184(1)	North Australian	Argyle	P	17	88	IaAB	1305	1284	1272	0.45
MwP1	Tanzanian	Mwadui	P	92	36	IaAB	1184	1166	1156	0.54
MwP2	Tanzanian	Mwadui	P	102	47	IaAB	1194	1176	1166	0.73
ArP1	North Australian	Argyle	P	50	8	IaA	1153	1136	1126	0.00
ArP2	North Australian	Argyle	P	0	NA	II	NA	NA	NA	0.23
ArE1	North Australian	Argyle	E	53	83	IaAB	1259	1239	1228	1.08
KFP1	Kaapvaal	Koffiefontein	P	102	65	IaAB	1214	1195	1185	1.80
KFP2	Kaapvaal	Koffiefontein	P	174	29	IaAB	1160	1143	1133	1.18
KFE1	Kaapvaal	Koffiefontein	E	587	68	IaAB	1171	1153	1143	0.19
KFE2	Kaapvaal	Koffiefontein	E	310	50	IaAB	1168	1150	1140	1.47
PrP1	Kaapvaal	Cullinan	P	48	78	IaAB	1252	1233	1222	0.50
PrE1	Kaapvaal	Cullinan	E	225	79	IaAB	1212	1193	1183	0.76
PrE2	Kaapvaal	Cullinan	E	499	100	IaB	NA	NA	NA	2.55
VeP1	Kaapvaal	Venetia	P	86	49	IaAB	1200	1182	1171	0.67
VeE1	Kaapvaal	Venetia	E	519	0	IaA	NA	NA	NA	0.04
OrP1	Zimbabwe	Orapa	P	114	40	IaAB	1184	1166	1156	0.17
OrP2	Zimbabwe	Orapa	P	106	54	IaAB	1200	1182	1171	0.07
OrE1	Zimbabwe	Orapa	E	120	39	IaAB	1181	1164	1153	0.16
OrE2	Zimbabwe	Orapa	E	83	32	IaAB	1183	1165	1155	0.32

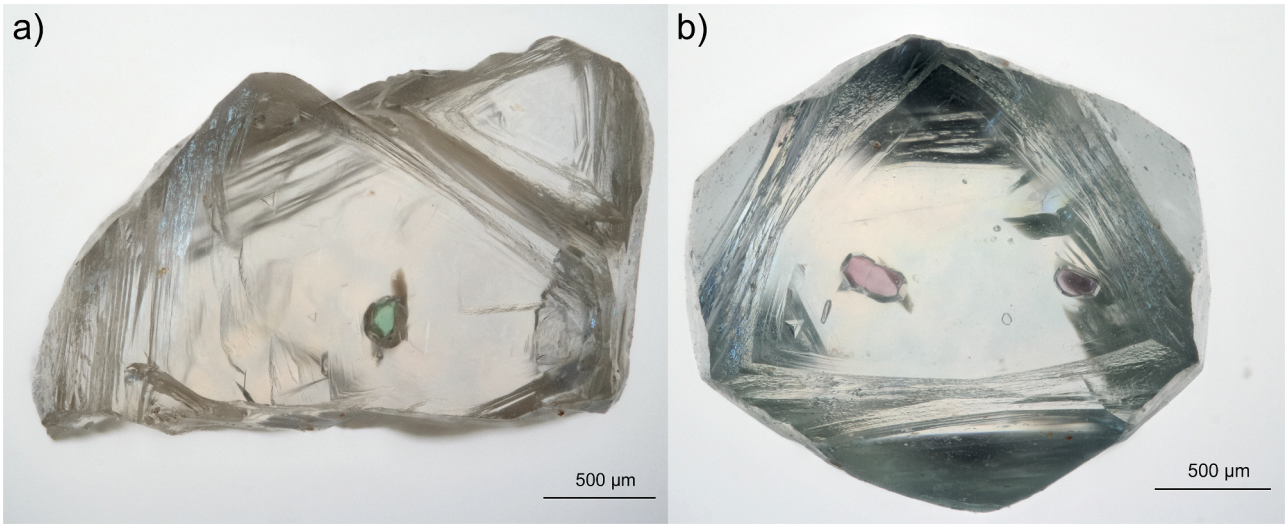

Fig. 1. Photos of two specimens analyzed in this study: (a) a broken macle twin with a green diopside inclusion (sample DBP1–1); (b) a greenish octahedral diamond with inclusions of purple peridotitic garnet (JwB33L6–2).

possible, single crystal X-ray diffraction (SC-XRD) was conducted. Analyses were performed with a Rigaku Oxford Diffraction SuperNova diffractometer equipped with a Dectris Pilatus 200K areal detector at the Dipartimento di Geoscienze (Padova). Monochromatized Mo Kα radiation (λ = 0.7107 Å) at 50 kV and 0.12 mA was used to conduct the measurements (sample-to-detector distance = 69 mm). Data reduction was performed with the CrysAlis Pro software (Rigaku Oxford Diffraction).

Sample VeB126P4–2, which showed an ambiguous signal in the Raman spectrum, produced a diffraction pattern consistent with exsolutions of orthopyroxene in a crystal of clinopyroxene. Similar exsolution features in clinopyroxene were reported for the first time by Leost et al. (2003).

2.4. X-ray computed tomography

X-ray CT was performed on all samples where an OH signal was observed in the IR spectra to identify possible fractures connecting inclusions to the surface of the diamond. This instrument was also used to precisely measure the thickness of the inclusions. Analyses were performed with a RX Solutions EasyTom equipped with an X-ray tube with a LaB_6 cathode operating at a voltage of 70 kV and a Varian PaxScan 2520DX imager at Laboratoire Magmas et Volcans (LMV, Université Clermont-Auvergne, Clermont-Ferrand, France). A 3D reconstruction of a garnet inclusion and an image section of a diamond are shown in Fig. 2.

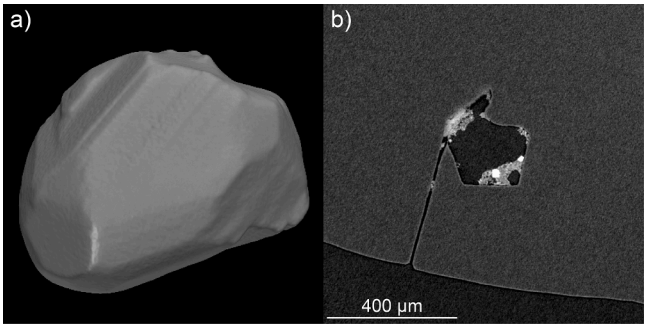

Fig. 2. (a) A 3D model of the garnet inclusion in sample Grt_E_4 reconstructed from X-ray CT, the inclusion is approximately 400 µm long in the longest direction. (b) An almost empty cavity partially filled with a multiphase material, note how the cavity is connected by a fracture to the surface of the diamond (sample FinB14).

The resolution of the X-ray CT was dependent on the size of the inclusions and diamonds, with voxel edge length of 1–2 µm, with only one sample having lower resolution data (2.4 µm for sample KFE2).

The thickness of mineral inclusions was calculated by computing the average of multiple measurements of the mineral in the propagation direction of the IR radiation to account for the irregular shape of some inclusions. X-ray CT also allowed recognition (and exclusion) of inclusions in contact with fractures in the diamond that could have allowed interaction with the surrounding mantle, thus modifying the composition and H_2O content of the inclusion after entrapment (Fig. 2b). Moreover, in some samples (e.g., DBP1–1), exsolutions of orthopyroxene in clinopyroxene inclusions were identified, although no exsolutions could be detected in sample VeB126P4–2 despite the opposite SC-XRD results described above.

2.5. Fourier-Transform infrared spectroscopy

FTIR spectra were recorded from diamonds to measure their N concentration and N-aggregation state, and from inclusions to measure their H_2O content. Analyses were performed using a Bruker Vertex 70 spectrometer with a globar IR source, a KBr beamsplitter and a liquid N_2 cooled MCT detector coupled with a Hyperion microscope with 15x objective at LMV (Clermont-Ferrand). Prior to analysis, diamonds were cleaned with ethanol in an ultrasonic bath for 15 min. Background spectra were collected through a CaF_2 window using 100 scans, sample spectra were collected using 300 scans at a spectral resolution of 2 cm^{-1}. Spectra of the diamond hosts were collected with unpolarized radiation and an aperture size that was adjusted to measure homogeneous and crack-free regions of each sample. Usually, five spectra were recorded from each diamond. Quantification of the N content and N-aggregation state was done by deconvolution by least-squares fitting of the N-region (i.e., ~1000 to 1400 cm^{-1}) of the diamond using the DiaMap Excel spreadsheet (Howell et al., 2012a; b). FTIR spectra were recorded where possible on mineral inclusions using an aperture size adjusted to enclose the entire inclusion whilst avoiding other inclusions and fractures. The H_2O content of the inclusions was determined by fitting the signal due to OH stretching bands between ~3000 and ~4000 cm^{-1}. The data processing consisted firstly of subtracting the spectrum of the diamond from that of the inclusion, because the signal due to diamond in the three-phonon region (Green et al., 2022) overlaps with the OH stretching region. After this step, the baseline of the resulting spectrum (of the inclusion only) was corrected using cubic spline fitting. Finally,

the integrated absorbance (area) of the OH stretching signal was calculated (Fig. 3).

The H_2O content of the mineral inclusions was calculated using absorption coefficients reported by Withers et al. (2012) for olivine, Bell et al. (1995) for orthopyroxene, peridotitic clinopyroxene, and garnet, and Koch-Müller et al. (2007) for eclogitic clinopyroxene.

Spectra were recorded from inclusions extracted from their diamond hosts using a Thermo Scientific Nicolet iN10 with an EverGlo air-cooled IR source, KBr beam splitter and liquid N_2 cooled MCT detector installed at the Dipartimento di Geoscienze (Padova). Spectra were collected with unpolarized radiation through a BaF_2 plate using 64 scans for both the background and spectrum at a spectral resolution of 4 cm^{-1}. Due to the small sizes, the extracted inclusions were not polished and spectra were recorded for different orientations of the same grain where possible and the resulting H_2O contents were averaged to calculate the final result. Baseline corrections were done using a cubic spline and the thickness was measured using an optical microscope with a precision of ±5 μm.

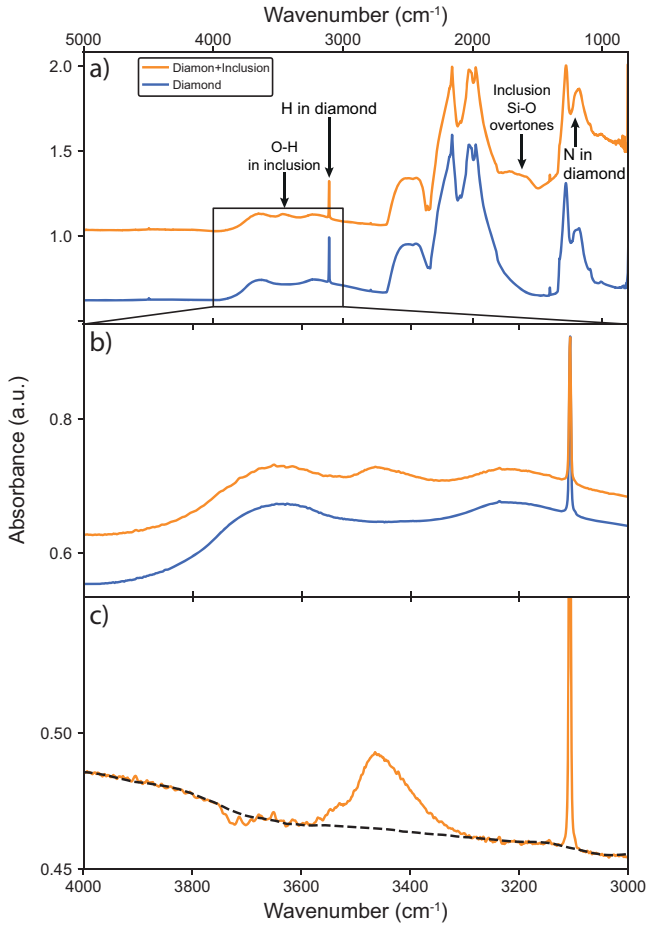

Fig. 3. Visual representation of the steps used to process spectra and to calculate the H_2O content of mineral inclusions (see text for more details). (a) Shows the FTIR spectra collected on a diamond and an inclusion within the diamond. (b) Shows an enlargement of (a) in the region between 3000 and 4000 cm^{-1}, the offset between the spectra in (b) was reduced to facilitate comparison of the spectra. (c) Shows the spectrum after subtraction of the contribution of the diamond (see text), the black dashed line represents the baseline used for that specific spectrum (sample JwB33B-2) such that the integrated area of the OH signal can be determined. The noise around ~3700 cm^{-1} in (c) is due to atmospheric water.

3. Results

3.1. Diamond N content and N-aggregation state

Nitrogen concentration in the diamonds studied here ranges from 0 (below FTIR detection which is approximately 10 at. ppm, see Day et al., 2023) to 950 at. ppm (Table 1, Fig. S2) with an average N content of 296 at. ppm. In five samples, the N signal in the one-phonon region was saturated and thus precise quantification of N content and N-aggregation state was not possible. However, fitting this saturated signal provided a lower estimate of N contents for these samples, which is always > 600 at. ppm.

Nitrogen is incorporated in diamond as isolated substitutional N atoms (C-centers). With progressive mantle annealing, C-centers aggregate to form A-centers, consisting of two neighboring N atoms, and then into B-centers, consisting of four N atoms surrounding a C vacancy (Green et al., 2022). According to the concentration of N and its aggregation state, diamond is classified as Type I (if it contains detectable amounts of N) and Type II (if it does not contain detectable amounts of N). Type II samples can be classified as IIa (if B is not detected) and IIb (if B is detected). Type I specimens can be further classified as Type Ib if N defects occur mainly as C-centers, or as Type Ia if N occurs in an aggregated form. Type Ia specimens are classified as IaA (> 90 % A-centers), IaAB (between 10 and 90 % A-centers) or IaB (< 10 % A-centers). Specimens are mostly Type Ia, with only 4 Type IIa samples, and no Type Ib or IIb sample are present. Type Ia diamonds are mainly Type IaAB (66 samples) with a small amount of IaA (3 samples) and IaB (2 samples). As the five samples with saturated N signals show signals due to both A- and B-centers, they were classified as Type IaAB although the exact A- and B-center content could not be determined.

The mantle residence temperature of each diamond was calculated using N-aggregation thermochronometry, following Leahy and Taylor (1997). The residence temperatures were calculated assuming three different residence times (1, 2 and 3 byr) and the results are reported in Table 1 and illustrated in Fig. S2. The highest and lowest residence temperatures in this database are 1305 °C (for 1 byr residence time) and 1078 °C (for 3 byr residence time), respectively, with an average between 1159 and 1188 °C, in agreement with the global average residence temperature of 1141–1174 °C (for peridotitic diamonds) and 1141–1168 °C (for eclogitic diamonds) for residence times of 3 and 1 byr, respectively (Stachel and Harris, 2008).

Out of all samples, 70 diamonds showed a sharp peak at 3107 cm^{-1} associated with H in the VN_3H^0 defect (Goss et al., 2014). The normalized linear absorbance (i.e., the peak height normalized to a sample thickness of 1 cm) of this peak was obtained using the DiaMap spreadsheet and is also reported in Table 1. Some samples with high N contents also showed a relatively weak peak at 3236 cm^{-1}, which has been tentatively attributed to H in the VN_4H^0 defect (Day et al., 2024).

3.2. H_2O in mineral inclusions

Four different OH stretching signals were identified in the FTIR spectra of the inclusions, which are described as follows. The first group (*Group 1* from here onwards) represents the most common case (107 samples) where, after subtraction of the diamond spectrum, a characteristic signal typical of OH stretching for silicate minerals, between 3000 and 4000 cm^{-1}, was observed (Table 2). In this case, the determination of the H_2O content of the mineral inclusion was straightforward (see Fig. 4). The second group (*Group 2*, 4 samples, see Table 2) consists of spectra that, after subtraction of the diamond spectrum, had a low signal/noise ratio and relatively weak signal due to OH stretching. This resulted in large uncertainties and prevented precise quantification of the low H_2O content of these minerals (Fig. S3a). The third group (*Group 3*, 3 samples, see Table 2) represents spectra where, after subtraction of the diamond spectrum, selecting a baseline was ambiguous and, consequently, only a range of H_2O contents could be determined

Table 2
Paragenesis, H_2O content (in ppm wt.) measured inside and outside the diamonds and abbreviated reference for the source of absorption coefficients used for H_2O quantifications for all mineral inclusions in this study.

Sample	Para	Phase	Calib	H_2O in	H_2O out	Sample	Para	Phase	Calib	H_2O in	H_2O out
Pr210–3	P	Cpx	B95	211	-	Grt_P_3	P	Grt	B95	9[2]	-
Pr210–3	P	Cpx	B95	126	-	Grt_P_4	P	Grt	B95	0[2]	-
DIO_01	P	Cpx	B95	0	-	JwB33L6–2	P	Grt	B95	0	-
DIO_02	P	Cpx	B95	12	-	JwB33L6–2	P	Grt	B95	0	-
DBP1–1	P	Cpx	B95	0–137[3]	-	MwP1	P	Grt	B95	0	-
DBP1–2	P	Cpx	B95	59	-	MwP2	P	Grt	B95	0	-
Wes1	P	Cpx	B95	0	24	MwP2	P	Grt	B95	0	-
KFB65P24	P	Cpx	B95	96	-	ArP2	P	Grt	B95	0	-
KFB65P24	P	Cpx	B95	46	-	KFP1	P	Grt	B95	0	-
VeB126P4–1-1	P	Cpx	B95	0	-	KFP1	P	Grt	B95	0	-
VeB126P4–2	P	Cpx	B95	61	168	KFP2	P	Grt	B95	0	-
ArB58T3184(1)	P	Cpx	B95	42	-	PrP1	P	Grt	B95	0	-
ECLO_2	E	Cpx	KM07	30	50	VeP1	P	Grt	B95	NA[4]	-
ECLO_2	E	Cpx	KM07	46	-	VeP1	P	Grt	B95	NA[4]	-
PR4	E	Cpx	KM07	451	-	OrP1	P	Grt	B95	0	-
V10_01	E	Cpx	KM07	141	-	OrP2	P	Grt	B95	0	-
V10_01	E	Cpx	KM07	54	-	Grt_E_2	E	Grt	B95	22	-
V10_02	E	Cpx	KM07	17–141[3]	-	Grt_E_2	E	Grt	B95	0	-
V10_03	E	Cpx	KM07	97	-	Grt_E_3	E	Grt	B95	0	-
DBP2–1	E	Cpx	KM07	55	-	Grt_E_3	E	Grt	B95	0	-
Dut1	E	Cpx	KM07	90	105	Grt_E_3	E	Grt	B95	0	-
FinB14	E	Cpx	KM07	65	-	Grt_E_3	E	Grt	B95	0	-
FinB15–2	E	Cpx	KM07	65	-	Grt_E_4	E	Grt	B95	550	471
KFB65P25	E	Cpx	KM07	241	223	FinB15–2	E	Grt	B95	NA[4]	-
VeB126P4–1-3	E	Cpx	KM07	80	-	FinB15P7	E	Grt	B95	0	-
Pr210–1	E	Cpx	KM07	0	-	FinB15P3	E	Grt	B95	0	-
Pr210–2	E	Cpx	KM07	58	-	Pr210–1	E	Grt	B95	0	-
Pr210–2	E	Cpx	KM07	170	-	Pr210–2	E	Grt	B95	0	-
Pr210–2	E	Cpx	KM07	170	-	Pr210–4	E	Grt	B95	0	-
Pr210–5	E	Cpx	KM07	0–195[3]	-	Pr210–4	E	Grt	B95	0	-
Pr210–5	E	Cpx	KM07	40	-	Pr210–6	E	Grt	B95	0	-
Pr210–5	E	Cpx	KM07	0	-	Pr210–8	E	Grt	B95	0	-
Pr210–9	E	Cpx	KM07	174	-	Pr210–10	E	Grt	B95	0[2]	-
Pr210–9	E	Cpx	KM07	0	-	Pr210–11	E	Grt	B95	0	-
Pr210–10	E	Cpx	KM07	285	-	JwB33B-1	E	Grt	B95	353	259
Pr210–10	E	Cpx	KM07	201	-	JwB33B-2	E	Grt	B95	0[2]	-
Pr210–11	E	Cpx	KM07	113	-	JwB34P	E	Grt	B95	0	-
OrB18P40–1	E	Cpx	KM07	200	-	LB18P68–1	E	Grt	B95	0	-
OrB18P40–1	E	Cpx	KM07	212	-	LB18P68–1	E	Grt	B95	0	-
OrB18P40–2	E	Cpx	KM07	25	-	LB18P68–2	E	Grt	B95	0	-
JwB33A-1	E	Cpx	KM07	0	-	LB18P68–2	E	Grt	B95	0	-
JwB33A-2	E	Cpx	KM07	63	-	Mw-1	E	Grt	B95	0	-
JwB33B-2	E	Cpx	KM07	95	-	UrP26	E	Grt	B95	0	-
JwB33B-2	E	Cpx	KM07	100	-	UrP26	E	Grt	B95	0	-
Mw-1	E	Cpx	KM07	105	-	UrP43	E	Grt	B95	0	-
Mw-4	E	Cpx	KM07	109	-	ArE1	E	Grt	B95	0	-
Mw-4	E	Cpx	KM07	112	-	ArE1	E	Grt	B95	0	-
KF2	P	Opx	B95	22	-	ArE1	E	Grt	B95	0	-
PR5	P	Opx	B95	10	-	KFE1	E	Grt	B95	0	-
PR5	P	Opx	B95	0	-	KFE1	E	Grt	B95	262	-
DIO_02	P	Ol	W12	4	-	KFE2	E	Grt	B95	0	-
KF4	P	Ol	W12	7	-	PrE1	E	Grt	B95	0	-
PM2	P	Ol	W12	0	-	PrE2	E	Grt	B95	0	-
PM2	P	Ol	W12	0	-	PrE2	E	Grt	B95	0	-
PM4	P	Ol	W12	7	-	VeE1	E	Grt	B95	0	-
ArP1	P	Ol	W12	0	-	OrE1	E	Grt	B95	0	-
						OrE2	E	Grt	B95	0	-
						VeP2	P	Grt	B95	NA[4]	-
						VeP3	P	Grt	B95	0	-
						ArE2	E	Grt	B95	0	-
						ArE3	E	Grt	B95	0	-

Para = Paragenesis; Calib = Calibration. B95 = Bell et al. (1995), KM07 = Koch-Müller et al. (2007), W12 = Withers et al. (2012). "H2O in" refers to the H2O content (in ppm wt.) measured inside the diamond; "H2O out" refers to the H2O content measured after release of the inclusion from the diamond host. [2] = Group 2, [3] = Group 3, [4] = Group 4, all other samples not maked by an apex belong to Group 1.

(Fig S3b). Finally, in the last group (*Group 4*, 4 garnet samples, see Table 2) the OH stretching region contains a sharp, intense band at a high frequency (~3695 cm^{-1}) characteristic of hydrous minerals (see e.g., Heller-Kallai et al., 1975), which may be present as micro/nano inclusions (Fig. S3c). This type of signal prevents precise quantification of H_2O content, but equilibration of the mineral in a H_2O-rich environment can be inferred nonetheless.

Only H_2O contents obtained from group 1 spectra are considered in the following discussions as they provide the most reliable quantifications. The analyzed inclusions span a wide range of H_2O contents from 0 (below the FTIR detection limit, which depends on sample size and measurement conditions) to 550 ppm wt. H_2O (Table 2, Fig. 5). The six olivine inclusions analyzed have low H_2O contents, ranging from 0 to 7 ppm wt., with an average H_2O content of 3 ppm wt., on the low end of

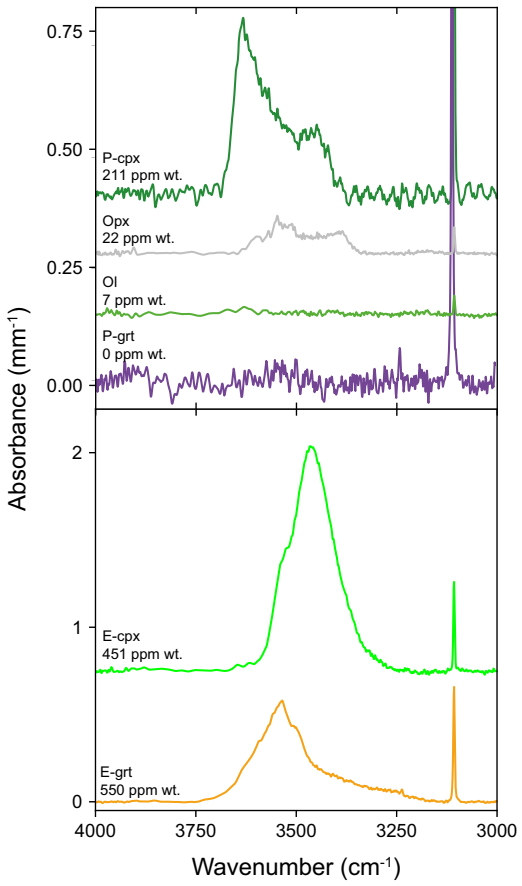

Fig. 4. FTIR spectra (after baseline correction and subtraction of the diamond spectrum) recorded from inclusions with the highest H_2O contents determined for each phase in this study. Absorbance was normalized to a thickness of 1 mm. The peak at 3107 cm^{-1} is due to the fundamental C-H stretching mode of the VN_3H^0 point defect in diamond (Goss et al., 2014). Cpx = clinopyroxene, Opx = orthopyroxenes, Ol = olivine, Grt = garnet. "P" and "E" refer to peridotitic and eclogitic paragenesis, respectively.

the range reported previously for olivine inclusions in diamonds (Fig. 5, i.e., Kurosawa et al., 1997; Matsyuk and Langer, 2004; Matveev and Stachel, 2009; Novella et al., 2015; Jean et al., 2016; Taylor et al., 2016; Bassoo and Befus, 2021; Vangu et al., 2023).

Only three orthopyroxene inclusions were analyzed and their H_2O content ranges from 0 to 22 ppm wt. with the average at 10 ppm wt., in agreement with data reported previously for orthopyroxene (Bassoo and Befus, 2021). It is important to note however, that the spectra recorded from olivine and orthopyroxene inclusions hosted in diamonds from Guyana studied by Bassoo and Befus (2021) show severe atmospheric contamination and poorly-constrained baseline corrections in some of their samples, which may have led to overestimation of H_2O contents. Therefore, data from olivine and orthopyroxene inclusions from Bassoo and Befus (2021) were excluded from subsequent discussions in this work.

Clinopyroxenes have high H_2O contents, with an average content of 97 ppm wt., and ranging from 0 to 451 ppm wt. (the latter being the highest H_2O content reported for a clinopyroxene inclusion in a diamond), in agreement with data reported in the literature (7–260 ppm wt. H_2O) by Taylor et al. (2016). Garnets are mostly dry, as previously observed (Matsyuk et al., 1998; Novella et al., 2015; Taylor et al., 2016). Note however that five inclusions from the present dataset belong to *Group 4*, suggesting that these garnets contain detectable amounts of OH. Moreover, three garnet outliers of eclogitic paragenesis (KFE1, JwB33B-1, and Grt_E_4) exhibit notable H_2O contents (>100 ppm wt.). The most H_2O-rich inclusion studied here is an eclogitic garnet (Grt_E_4, which belongs to *Group 1*) from the Udachnaya mine (Siberian craton, Russia), which showed a broad absorption band from ~3000 to ~3750 cm^{-1} with a superimposed band at ~3535 cm^{-1}. A similar spectrum was reported by Geiger et al. (1991) for a synthetic garnet hosting fluid inclusions. In fact, Grt_E_4 also exhibits a band around 1600 cm^{-1}, representative of the H_2O bending mode, which indicates the presence of fluid or melt nano inclusions that were not detectable with X-ray CT. Determination of H_2O content for this sample was performed after subtraction of the broad band between ~3000 and ~3700 cm^{-1} attributed to OH stretching of the H_2O molecules associated with fluid inclusions, as done by Geiger et al. (1991). Following this approach, 550 ppm wt. H_2O were calculated for the structurally bound OH in the garnet, which is the highest H_2O content ever reported for a garnet inclusion in a diamond, and one of the highest for cratonic mantle garnets in general.

The inclusions extracted from their diamond hosts include three

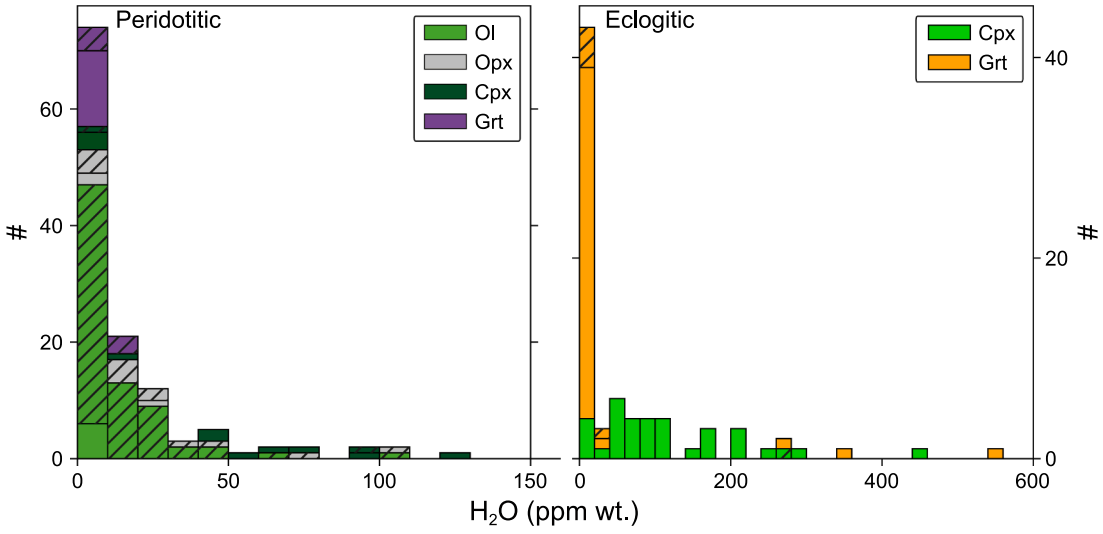

Fig. 5. Distribution of H_2O content in peridotitic and eclogitic mineral inclusions from lithospheric diamonds. Hatched patterns represent H_2O contents from the literature. The bin size for the peridotitic histogram is 10 ppm wt., while for the eclogitic histogram is 20 ppm wt. Cpx = clinopyroxene, Opx = orthopyroxenes, Ol = olivine, Grt = garnet.

omphacites, two diopsides and two eclogitic garnets. The H_2O contents of these minerals, measured inside and outside the diamond, agree within ±30 % (see Table 2 and discussion below), confirming the validity of H_2O quantifications of mineral inclusions determined while still inside the diamonds.

4. Discussion

4.1. Validation of H_2O contents of mineral inclusions

There are several errors associated with collecting the FTIR spectra of mineral inclusions inside diamonds that need to be considered to accurately derive H_2O contents from such spectra. (i) Firstly, recording FTIR spectra of inclusions through the diamond host decreases the ratio of absorption signal from OH in the inclusion to noise (i.e., the inclusion signal-to-noise ratio), especially in large diamonds. This makes H_2O quantification particularly challenging for inclusions with low H_2O contents that show relatively weak signal due to OH stretching modes which is hard to differentiate from noise (i.e., *Group 2* spectra, see Section 3.4). (ii) Another important source of error is related to the determination of the thickness of the inclusions. In this study, thickness was calculated assuming that the IR radiation passed through the whole volume of the inclusion as the size of the IR aperture was set, where possible, such that it enclosed the entire inclusion. However, the high refractive index of diamond (Edwards and Ochoa, 1981) prevents precise determination of the optical path and of the volume traversed by IR radiation, introducing errors in the quantification of the thickness of inclusions. (iii) The procedure used to process each spectrum (see Section 2.5) may also result in errors on the measured H_2O contents. Variability in the position and intensity of broad-peaks in the diamond three-phonon region is common when comparing the spectra of different diamonds and is even observed when comparing spectra recorded from different regions of the same diamond. During subtraction of the diamond spectrum from each IR spectra (recorded through the inclusion and diamond), such variability in the three-phonon region between 3000 and 4000 cm^{-1} can produce artefacts that may be mistaken for OH stretching signal (*Group 3* signals). Baseline subtraction can also introduce errors, especially for spectra recorded from samples with relatively low H_2O contents where the distinction between signal and baseline is not clear. (iv) Moreover, the use of unpolarized radiation to measure a single unoriented section of an anisotropic mineral inclusion also contributes to the error, however, this is unavoidable as reliable orientation of inclusions inside the diamond is extremely challenging. (v) Lastly, inclusions often break in the process of release from their host, and only part of them can be recovered and analyzed, and this could also introduce some uncertainty in analyses outside the diamonds as only a fraction of inclusion (which may not be representative of the whole sample) is analyzed.

As all sources of error described above are associated with recording FTIR spectra of the inclusions through diamond, the error was determined by comparing H_2O contents obtained from spectra recorded from inclusions inside their diamond host and then from the same inclusions once they were extracted. The H_2O contents measured from inclusions inside and outside the diamond agree within ±30 % (Fig. 6), and a similar error is reported in other studies (e.g., 30–50 % by Novella et al. (2015). Two samples show an error larger than ±30 %, VeB126P4–2 and Wes1. VeB126P4–2 is a combination of clinopyroxene/orthopyroxene exsolutions which broke during extraction. This difference is likely due to sampling different of ortho- and clinopyroxene by the IR beam. No H_2O was detected in sample Wes1 measured inside the diamond, and this is likely due to relatively low H_2O content measured outside.

4.2. H_2O in inclusions in diamonds vs xenoliths

Inclusions in diamonds in this study show a relationship between their H_2O content and paragenesis. Eclogitic clinopyroxenes show maximum and average H_2O contents of 451 and 110 ppm wt., respectively, while peridotitic clinopyroxenes show maximum and average H_2O contents of 211 and 61 ppm wt., respectively (Fig. 7).

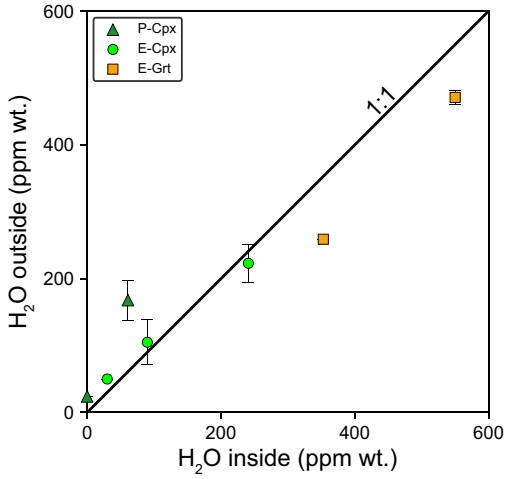

Fig. 6. Comparison of H_2O contents obtained for the same inclusions inside and outside of their diamond host. The colors correspond to the spectra of different inclusion phases as shown in Fig. 4. The error bars represent the standard deviation calculated from different H_2O quantifications on different pieces of the inclusions, or on different orientations of the same crystal.

The same general trend is observed for garnets, although it is more complex. Peridotitic garnets are always dry, except for the samples with *Group 4* spectra (3 in total). These samples likely host some amount of H_2O, and the nano inclusions of hydrous phases may have formed from exsolution caused by H_2O saturation during decompression and cooling of the sample. It follows that at high P and T, these garnets could have hosted significant amounts of structurally bound H_2O. Eclogitic garnets are also mostly dry, but three outliers with H_2O contents >100 ppm wt., as well as one sample from *Group 4*, are present (Fig. 7), suggesting that on average eclogitic garnet contains more H_2O than peridotitic garnet, in agreement with observations from xenoliths (Fig. 7).

The more hydrated nature of the eclogitic mantle, compared to its peridotitic counterpart, is shown here for the first time based on data from mineral inclusions in diamonds, confirming prior observations made for (possibly) metasomatized xenoliths. This H_2O enrichment in eclogites is not surprising as they are derived from subducted oceanic crust, which is a more H_2O-rich environment compared to the peridotitic ambient mantle. The preferential incorporation of H_2O in eclogites is also related to mineral composition, where the presence of Al in clinopyroxene promotes H incorporation (O'Leary et al., 2010), causing eclogitic (Al-rich) clinopyroxenes to have a higher H_2O mineral/melt partition coefficient compared to their peridotitic (Al-poor) counterparts (see e.g., Aubaud et al., 2008; Novella et al., 2014).

Inclusions in diamonds have lower H_2O contents than their xenolithic equivalents. This discrepancy may be due to of the following: (i) sampling bias as most diamonds in this study and the literature come from the Kaapvaal and Siberian cratons and are compared to data from a worldwide suite of xenoliths. Overrepresentation of these two diamond localities could skew the distribution to lower average H_2O contents. However, this does not seem to be the case as xenoliths from the Kaapvaal and Siberian cratons exclusively, still show a higher average H_2O content (Fig. S4). (ii) Metasomatism subsequent to diamond formation, as previously described in the literature (Doucet et al., 2014; Demouchy and Bolfan-Casanova, 2016). However, some studies report high H_2O contents for minerals in pristine xenoliths (see e.g., Moine et al., 2020; Aulbach et al., 2023). Moreover, it was recently shown for eclogitic xenoliths from Africa that metasomatic alteration does not necessarily result in H_2O-enrichment (Aulbach et al., 2024). It follows

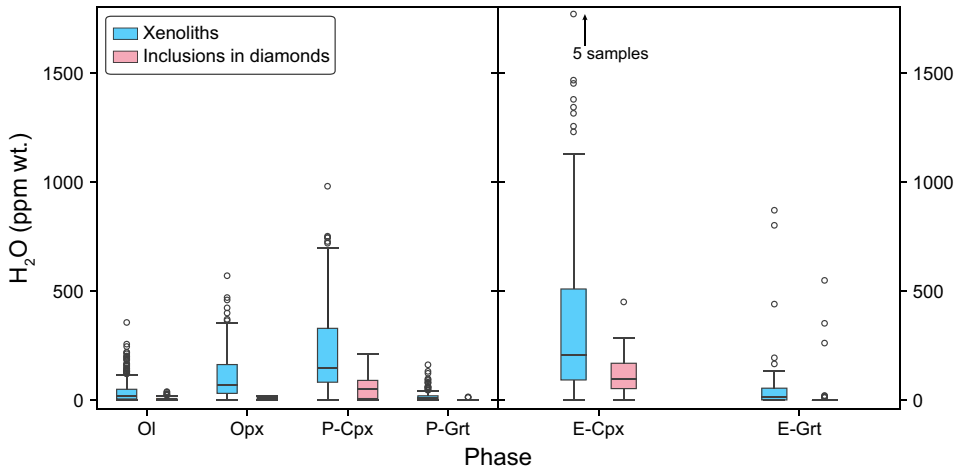

Fig. 7. Boxplot of the H_2O content measured in minerals in xenoliths (> 1700 samples from a worldwide database) and in inclusions in diamonds (left and right, respectively). For clarity, the vertical axis was cut leaving five samples outside of the plot. The box represents the data interval between the first (Q1) and third (Q3) quartiles of the distribution, the horizontal line in the box represents the median. The whiskers represent the tails of the distribution, and the dots are outliers defined as falling outside Q1–1.5*IQR and Q3+1.5*IQR (IQR = interquartile range). For details regarding the source of H_2O data from xenoliths see Appendix I.

that metasomatism might play a role in enriching xenoliths in H_2O compared to inclusions in diamond, but it is unlikely to be the main/-only factor causing the difference in H_2O content. (iii) The H_2O content of mineral inclusions does not reflect that of the average cratonic lithosphere. Diamonds are the result of localized metasomatic events. Therefore, the inclusions they host may be different from the same minerals in different areas of the cratonic lithosphere that are not affected by the type of metasomatism required for diamond formation. If the diamond forming medium is characterized by a low H_2O activity (a_{H_2O}) the diamond-hosted mineral inclusions will show a lower H_2O content than the same minerals in area of the lithosphere not interested by diamond growth.

4.3. Source of H_2O in mineral inclusions in diamonds

Mineral inclusions in diamonds may either be protogenetic (i.e., formed before their diamond host) or syngenetic (i.e., formed at the same time as their diamond host). Arguments in favor of both syngenesis (Bulanova, 1995; Wiggers de Vries et al., 2011) and protogenesis (Thomassot et al., 2009; Nestola et al., 2017) have been proposed, however, there is growing body of evidence supporting the latter (see Bruno et al., 2024). Consequently, we can initially assume the inclusions studied here are protogenetic and therefore their H_2O content is either primary, representative of the H_2O content of the minerals in the mantle before diamond formation, or reflects equilibration of the mineral with the diamond forming medium during diamond growth. The latter scenario is possible due to the high diffusivity of H in silicates (see Ingrin and Blanchard, 2006, and references therein). To investigate this possibility by quantifying the diffusivity of H, a diffusion model was constructed for olivine, orthopyroxene, garnet and clinopyroxene at P/T conditions conducive to diamond formation by solving Fick's second law of diffusion (details regarding the boundary conditions, parameters and solution used for the modelling are given in Appendix II). The resultant diffusion profiles (Figs. 8, S5 and S6) confirm that H equilibration in NAMs at temperatures characteristic of diamond formation (i.e., 1000–1200 °C) is extremely fast. For example, the H_2O content of a 500 μm long garnet (the mineral with the lowest diffusivity among those considered and with a size significantly larger than the average size of

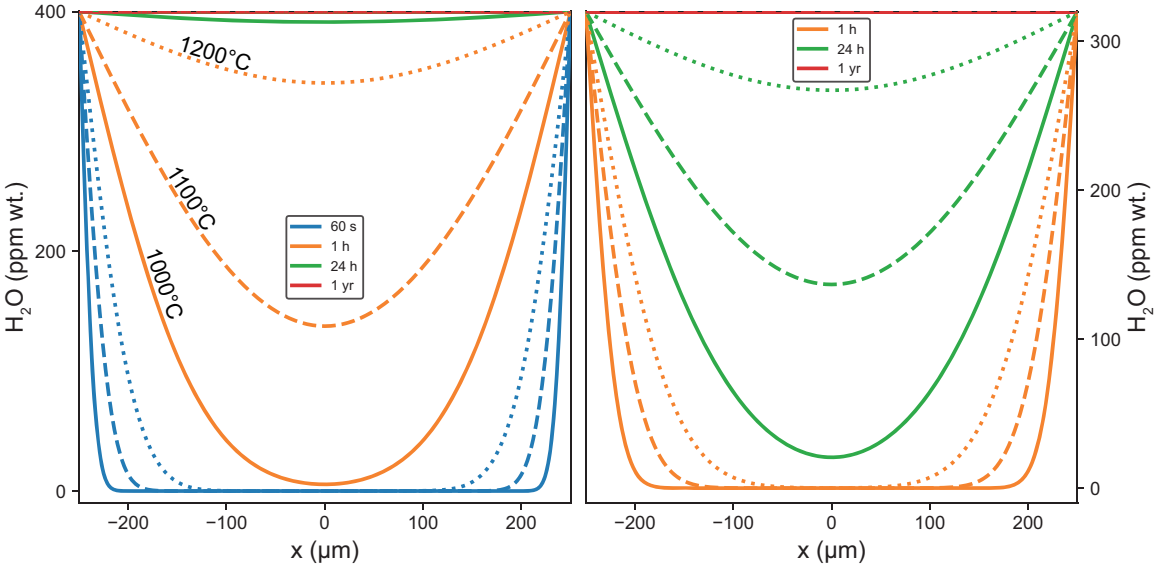

Fig. 8. Diffusion profiles of H_2O at different times and temperatures for olivine (left) and garnet (right). For details regarding the diffusion profiles calculations and the parameters used see Appendix II.

inclusions observed here) will completely re-equilibrate in about seven days, with other minerals generally requiring less than 24 h. Although the time required for a diamond to form in the mantle remains uncertain, diamond growth is unlikely to occur in the timespan of minutes or hours (Gress et al., 2018), implying that the H_2O content of mineral inclusions in diamonds most likely reflects the H_2O content of the diamond forming medium. Similar metasomatic re-equilibration between mantle substrate and metasomatic fluids was already described for major elements by Mikhail et al. (2021).

In this regard, the initial assumption of protogenesis becomes irrelevant, as the H_2O content of inclusions is related to that of the diamond forming medium both in the case of syngenesis (i.e. simultaneous formation of the inclusion and diamond from the same medium) and protogenesis (i.e. re-equilibration of H_2O between the inclusion and the diamond forming medium).

As it is likely that the H_2O in NAMs completely re-equilibrates with the diamond forming medium, diffusive loss of H from the inclusion after diamond formation could in principle occur. Matveev & Stachel (2009) explained the dry nature of olivine inclusions in diamonds from Ghana and Canada by escape of H from the inclusion to the mantle, following experiments suggesting high H diffusion in diamond by Popovici et al. (1995). However, it is important to carefully assess this possibility since high H diffusivities in diamonds do not necessarily imply that H can leave the inclusion, effectively cross the inclusion-diamond interface, and then pass through the diamond and enter the surrounding mantle. In fact, Vangu et al. (2023) measured different H contents in cuboid and octahedral sectors of an asteriated diamond and attribute this to a lack of H diffusion between sectors. For diffusion of H from the inclusion to the mantle to occur, a chemical gradient would be required. To remove H from the inclusions, a low a_{H_2O} would be required in the surrounding mantle, and if this was the case, then H would escape from all diamonds (if not trapped by N-related defects) and all inclusions, assuming equilibration. This is, however, not the case, as H_2O-bearing inclusions exist (as shown) and H commonly occurs as an impurity in diamond (e.g., Day et al., 2024). Moreover, since minerals in xenoliths are generally more H_2O-rich than inclusions in diamond, even for xenoliths that have not been metasomatized, an imposed chemical gradient would be opposite of that required for diffusive loss of H from the inclusion. Instead, this gradient would promote diffusion of H into the inclusion from the mantle, increasing H_2O content of the inclusion after diamond formation. However, this scenario also appears to be inoperative given the fact that dry inclusions are observed. Another important observation is that in N-bearing diamonds (most diamonds reported in this study and in general, Cartigny et al., 2022b), H tends to be associated with N and vacancy (V)-related defects, as evidenced by IR peaks observed at 3107 (VN_3H^0) and 3236 cm^{-1} (VN_4H^0). In fact, any point defect that involves substitutional N results in uncoupled electrons on adjacent C atom(s) that act to trap H via passivation of dangling C bonds. As the major N defects (i.e., C-, A-, or B- centers) involve substitutional N it is likely that H will be trapped by N, thus minimizing diffusive loss of H from diamonds of any aggregation state. The situation is different for Type IIa diamonds that contain N in concentrations below the FTIR detection limit, however, four inclusions contain H_2O in these diamonds, implying that significant loss of H is unlikely.

Combining all the above observations, it seems reasonable to assume that H will not escape the inclusion after diamond formation, and instead the H_2O content of the inclusion will be preserved after re-equilibration with the diamond forming medium.

4.4. H_2O and the diamond forming medium

In the previous section, it is argued that the H_2O content of NAM inclusions in diamonds reflects re-equilibration of pre-existing mantle minerals with the diamond forming medium during diamond formation. If equilibrium is achieved, through fast H diffusion, the H_2O content in the mineral can be related to the H_2O content of the diamond forming medium. The diamond forming medium may be a melt or a fluid (i.e., high-density supercritical fluids and low-density fluids, Weiss et al., 2022).

i) *Melts:* the H_2O content of the inclusions will be related to that of the melt according to H_2O mineral/melt partition coefficients ($Kd_{H_2O}^{min/melt}$). By using the average H_2O content of olivine, pyroxene and garnet inclusions in diamonds (from this study and the literature), together with $Kd_{H_2O}^{min/melt}$ measured in high-pressure high-temperature experiments (Aubaud et al., 2008; Novella et al., 2014), a range of H_2O contents expected for diamond forming melts is calculated. For peridotitic diamond forming melts, H_2O contents of 0.07 to 0.5 wt% in the melt are estimated, similar to the H_2O content proposed by Novella et al. (2015) based on olivine and garnet inclusions in diamonds from the Udachnaya kimberlite (0.09 wt% H_2O). For eclogitic diamond forming melts, on the other hand, H_2O contents of 0.5 to 1.5 wt% are expected. To precipitate diamond, the melt must be C-rich, and the presence of C has been shown to lower $Kd_{H_2O}^{min/melt}$ (Sokol et al., 2013). Consequently, in a C-rich melt, H_2O will be more incompatible in NAMs, and a higher H_2O content in the melt would be required to equilibrate inclusions with H_2O contents like those measured here. Experimental work shows that, at least for olivine, $Kd_{H_2O}^{min/melt}$ is halved in systems with very high C contents (Sokol et al., 2013), implying that the H_2O content of diamond forming media could be approximately twice that reported above (between 0.14 and 3 wt%). The H_2O contents reported here were calculated using the average H_2O contents of the inclusions but almost identical values are produced even when the highest reported H_2O contents are considered. The only exceptions are the two H_2O-rich eclogitic garnets reported in this study, specifically Grt_E_4 (471 ppm wt. H_2O), which requires equilibration with a melt with ~26 wt% H_2O (if no CO_2 is present), suggesting diamond-formation in a different, extremely H_2O-rich, environment compared to what is observed from other inclusions. The H_2O content of diamond forming melts calculated here is in agreement with modelling of hydrous low-degree melts that can form in the convective upper mantle (see Appendix III and Fig. S7).

This model is valid for hydrous-carbonated silicate melts, however, carbonatitic melts may also be involved in diamond formation (e.g., Weiss et al., 2022). The H_2O mineral/melt partition coefficients nor the H_2O activity-composition relationship for carbonatitic melts has been determined and therefore modelling them based on the H_2O content of the mineral inclusions is not possible. These melts could still be compatible with the H_2O contents measured in the mineral inclusions because of the low a_{H_2O} in carbonatites suggested by the markedly higher H_2O solubility in carbonatites compared to silicate melts (Keppler, 2003).

ii) *Fluids:* diamond forming fluids can either be supercritical high-density fluids described as brines (see Weiss et al., 2022) or low-density C-O-H fluids (Stachel and Harris, 2009). Both types of fluids may be compatible with the low H_2O contents of mineral inclusions if a_{H_2O} is low. This can occur due to interaction of H_2O with C (e.g., Yang et al., 2014) or other chemical species dissolved in the fluids that can lower the activity coefficient of H_2O (to values lower than those relevant for silicate melts), thus resulting in equilibration of inclusions with low H_2O contents. Alternatively, highly reducing conditions (such that a CH_4-rich fluid would be stable) would drastically decrease a_{H_2O} in the fluids by stabilizing CH_4 and H_2 (Frost and McCammon, 2008) and would also result in low H_2O contents in minerals equilibrated with such fluids. Unfortunately, no data are available regarding the activity coefficients and activity-composition relationships of these fluids, and therefore modelling their composition and H_2O content based on data from diamond-hosted mineral inclusions is not possible.

5. Conclusions

In this study the H_2O content of 118 NAM inclusions hosted in monocrystalline diamonds was measured with FTIR spectroscopy. The results show that:

- Eclogitic mineral inclusions contain more H_2O than peridotitic inclusions, implying a higher H_2O content in eclogitic environments related to diamond formation.
- NAM inclusions in diamonds have a lower H_2O content than the same minerals in mantle xenoliths, this is attributed to (i) a sampling bias, (ii) metasomatism subsequent to diamond formation, (iii) low a_{H_2O} in the diamond-forming environment.
- The H_2O content of NAM inclusions reflects equilibration with the diamond forming medium which, at equilibrium, is controlled by the H_2O partition coefficient.
- Significant H loss from the inclusion is unlikely due to unrealistic chemical gradients between the mantle and the inclusion and the presence of several barriers mitigating diffusive loss of H from the inclusion to the mantle (e.g., H trapped by vacancy and N-related defects).
- Diamond forming media associated with the formation of lithospheric monocrystalline diamond may be described as silicate melts with a relatively low H_2O content ($\leq$ 3 wt%) or carbonatitic melts or fluids with a low H_2O activity.

Data availability

Data can be accessed from the University of Padova online repository at https://researchdata.cab.unipd.it/id/eprint/1517.

Funding

This is contribution no. 690 of the ClerVolc program of the International Research Center for Disaster Sciences and Sustainable Development of the University of Clermont Auvergne, supported by the Agence Nationale de la Recherche. The Graduate Track of Involc is also thanked for funding visiting of A.C. at LMV. D.N. thanks the Rita Levi Montalcini program for support. This work was supported by the European Union (ERC, INHERIT, Strating Grant No. 101041620). Views and opinions expressed are, however, those of the author(s) only and do not necessarily reflect those of the European Union or the European Research Council Executive Agency. Neither the European Union nor the granting authority can be held responsible for them.

CRediT authorship contribution statement

Andrea Curtolo: Writing – original draft, Visualization, Software, Methodology, Investigation, Formal analysis, Data curation, Conceptualization. **Maxwell C. Day:** Writing – review & editing, Validation. **Francesca Innocenzi:** Writing – review & editing. **Nathalie Bolfan-Casanova:** Writing – review & editing, Validation, Supervision, Funding acquisition. **Martha G. Pamato:** Writing – review & editing, Funding acquisition. **Simon Falvard:** Writing – review & editing, Investigation. **Fabrizio Nestola:** Writing – review & editing, Investigation. **Jeff W. Harris:** Writing – review & editing, Resources. **Davide Novella:** Writing – review & editing, Supervision, Conceptualization.

Declaration of competing interest

The authors confirm that this work is original and has not been published elsewhere, nor is it currently under consideration for publication elsewhere. *Use of generative AI*. No artificial intelligence tools or services were used to write, construct or organize any part of this manuscript.

Acknowledgments

The authors thank James Badro for editorial handling as well as Thomas Stachel and Hans Keppler for providing helpful reviews that greatly improved the quality of this manuscript.

Supplementary materials

Supplementary material associated with this article can be found, in the online version, at doi:10.1016/j.epsl.2025.119311.

References

Aines, R.D., Rossman, G.R., 1984. Water content of mantle garnets. Geology 12 (12), 720. https://doi.org/10.1130/0091-7613(1984)12. <720:WCOMG>2.0.CO;2.

Aubaud, C., Hirschmann, M.M., Withers, A.C., Hervig, R.L., 2008. Hydrogen partitioning between melt, clinopyroxene, and garnet at 3 GPa in a hydrous MORB with 6 wt.% H2O. Contrib. Mineral. Petrol. 156 (5), 607–625. https://doi.org/10.1007/s00410-008-0304-2.

Aulbach, S., Stalder, R., Massuyeau, M., Stern, R.A., Ionov, D.A., Korsakov, A.V., 2023. Water in omphacite and garnet from pristine xenolithic eclogite: t-X-fO2 controls, retentivity, and implications for electrical conductivity and deep H2O recycling. Geochemistry, geophysics. Geosystems 24 (12). https://doi.org/10.1029/2023GC011170.

Aulbach, S., Gies, N.B., Linckens, J., Stalder, R., Viljoen, F., 2024. Inhibited hydrogen uptake in metasomatised cratonic eclogite. Contrib. Mineral. Petrol. 179 (8), 77. https://doi.org/10.1007/s00410-024-02157-6.

Aulbach, S., Harris, J.W., Stachel, T., 2022a. Mineral inclusions in lithospheric diamonds. In: Stachel, T., Smit, K., Shirey, S., Pearson, G., Nestola, F., Moses, T. (Eds.), Diamond: Genesis, Mineralogy and Geochemistry. Mineralogical Society of America, pp. 307–391. https://doi.org/10.2138/rmg.2022.88.06.

Bassoo, R., Befus, K.S., 2021. Composition of the Sub-Cratonic mantle of the Guiana Shield inferred from diamond-hosted inclusions. Geochem. Geophys. Geosyst. 22 (6). https://doi.org/10.1029/2021GC009841 e2021GC009841.

Bell, D.R., Rossman, G.R., 1992a. The distribution of hydroxyl in garnets from the subcontinental mantle of Southern Africa. Contrib. Mineral. Petrol. 111 (2), 161–178. https://doi.org/10.1007/BF00348949.

Bell, D.R., Rossman, G.R., 1992b. Water in Earth's mantle: the role of nominally anhydrous minerals. Science 255 (5050), 1391–1397. https://doi.org/10.1126/science.255.5050.1391.

Bell, D.R., Ihinger, P.D., Rossman, G.R., 1995. Quantitative analysis of trace OH in garnet and pyroxenes. Am. Mineral. 80 (5–6), 465–474. https://doi.org/10.2138/am-1995-5-607.

Bruno, M., Ghignone, S., Aquilano, D., Nestola, F., 2024. A critique of using epitaxial criterion to discriminate between protogenetic and syngenetic mineral inclusions in diamond. Sci. Rep. 14 (1), 8674. https://doi.org/10.1038/s41598-024-59432-6.

Bulanova, G.P., 1995. The formation of diamond. J. Geochem. Explor. 53 (1–3), 1–23. https://doi.org/10.1016/0375-6742(94)00016-5.

Cartigny, P., Chacko, T., Pearson, D.G., Stachel, T., 2022b. Carbon and nitrogen in mantle-derived diamonds. In: Stachel, T., Smit, K., Shirey, S., Pearson, G., Nestola, F., Moses, T. (Eds.), Diamond: Genesis, Mineralogy and Geochemistry. Mineralogical Society of America, pp. 809–875. https://doi.org/10.2138/rmg.2022.88.15.

Chin, E.J., Chilson-Parks, B., Boneh, Y., Hirth, G., Saal, A.E., Hearn, B.C., Hauri, E.H., 2021. The peridotite deformation cycle in cratons and the deep impact of subduction. Tectonophysics 817, 229029. https://doi.org/10.1016/j.tecto.2021.229029.

Curtolo, A., Novella, D., Logvinova, A., Sobolev, N.V., Davies, R.M., Day, M.C., Pamato, M.G., Nestola, F., 2023. Petrology and geochemistry of Canadian diamonds: an up-to-date review. In Earth Sci. Rev. 246. https://doi.org/10.1016/j.earscirev.2023.104588. Elsevier B.V.

Day M.C., Pamato M.G., Novella D., & Nestola F. (2023). Imperfections in natural diamond: the key to understanding diamond genesis and the mantle. In Rivista del Nuovo Cimento. Springer Science and Business Media Deutschland GmbH. 10.1007/s40766-023-00045-6.

Day, M.C., Jollands, M.C., Novella, D., Nestola, F., Dovesi, R., Pamato, M.G., 2024. Hydrogen-related defects in diamond: a comparison between observed and calculated FTIR spectra. Diam. Relat. Mater. 143, 110866. https://doi.org/10.1016/j.diamond.2024.110866.

Demouchy, S., Bolfan-Casanova, N., 2016. Distribution and transport of hydrogen in the lithospheric mantle: a review. Lithos 402–425. https://doi.org/10.1016/j.lithos.2015.11.012, 240–243.

Doucet, L.S., Peslier, A.H., Ionov, D.A., Brandon, A.D., Golovin, A.V., Goncharov, A.G., Ashchepkov, I.V., 2014. High water contents in the Siberian cratonic mantle linked to metasomatism: an FTIR study of Udachnaya peridotite xenoliths. Geochim. Cosmochim. Acta 137, 159–187. https://doi.org/10.1016/j.gca.2014.04.011.

Edwards, D.F., Ochoa, E., 1981. Infrared refractive index of diamond. J. Opt. Soc. Am. 71 (5), 607–608.

Frost, D.J., McCammon, C.A., 2008. The redox State of Earth's mantle. Annu Rev. Earth Planet. Sci. 36, 389–420. https://doi.org/10.1146/annurev.earth.36.031207.124322.

Geiger, C.A., Langer, K., Bell, D.R., Rossman, G.R., Winkler, B., 1991. The hydroxide component in synthetic pyrope. Am. Mineral. 76 (1–2), 49–59.
Goss, J.P., Briddon, P.R., Hill, V., Jones, R., Rayson, M.J., 2014. Identification of the structure of the 3107 cm −1 H-related defect in diamond. J. Phys. Condens. Matter 26 (14), 145801. https://doi.org/10.1088/0953-8984/26/14/145801.
Green, D.H., 1973. Experimental melting studies on a model upper mantle composition at high pressure under water-saturated and water-undersaturated conditions. Earth Planet. Sci. Lett. 19 (1), 37–53. https://doi.org/10.1016/0012-821X(73)90176-3.
Green, B.L., Collins, A.T., Breeding, C.M., 2022. Diamond spectroscopy, defect centers, color, and treatments. In: Smit, K., Shirey, S., Pearson, G., Stachel, T., Nestola, F., Moses, T. (Eds.), Diamond: Genesis, Mineralogy and Geochemistry. Mineralogical Society of America, pp. 637–688. https://doi.org/10.2138/rmg.2022.88.12, 1.
Gress, M.U., Howell, D., Chinn, I.L., Speich, L., Kohn, S.C., van den Heuvel, Q., Schulten, E., Pals, A.S.M., Davies, G.R., 2018. Episodic diamond growth beneath the Kaapvaal Craton at Jwaneng Mine, Botswana. Mineral. Petrol. 112 (S1), 219–229. https://doi.org/10.1007/s00710-018-0582-y.
Heller-Kallai, L., Yariv, Sh., Gross, S., 1975. Hydroxyl-stretching frequencies of serpentine minerals. Mineral. Mag. 40 (310), 197–200. https://doi.org/10.1180/minmag.1975.040.310.09.
Hirth, G., Kohlstedt, D., 2003. Rheology of the upper mantle and the mantle wedge: a view from the experimentalists. In: Eiler, J. (Ed.), Inside the Subduction Factory. American Geophysical Union, pp. 83–105. https://doi.org/10.1029/138GM06.
Howell, D., O'Neill, C.J., Grant, K.J., Griffin, W.L., Pearson, N.J., O'Reilly, S.Y., 2012a. μ-FTIR mapping: distribution of impurities in different types of diamond growth. Diam. Relat. Mater. 29, 29–36. https://doi.org/10.1016/j.diamond.2012.06.003.
Howell, D., O'Neill, C.J., Grant, K.J., Griffin, W.L., O'Reilly, S.Y., Pearson, N.J., Stern, R. A., Stachel, T., 2012b. Platelet development in cuboid diamonds: insights from micro-FTIR mapping. Contrib. Mineral. Petrol. 164 (6), 1011–1025. https://doi.org/10.1007/s00410-012-0786-9.
Ingrin, J., Blanchard, M., 2006. Diffusion of hydrogen in minerals. In: Keppler, H., Smyth, J.R. (Eds.), Water in Nominally Anhydrous Minerals. De Gruyter, pp. 291–320. https://doi.org/10.2138/rmg.2006.62.13.
Jackson, C.G., Gibson, S.A., 2023. Build-up of multiple volatiles in Earth's continental keels: implications for craton stability. Earth Planet. Sci. Lett. 611, 118134. https://doi.org/10.1016/j.epsl.2023.118134.
Jean, M.M., Taylor, L.A., Howarth, G.H., Peslier, A.H., Fedele, L., Bodnar, R.J., Guan, Y., Doucet, L.S., Ionov, D.A., Logvinova, A.M., Golovin, A.V., Sobolev, N.V., 2016. Olivine inclusions in Siberian diamonds and mantle xenoliths: contrasting water and trace-element contents. Lithos 265, 31–41. https://doi.org/10.1016/j.lithos.2016.07.023.
Keppler, H., 2003. Water solubility in carbonatite melts. Am. Mineral. 88 (11–12), 1822–1824. https://doi.org/10.2138/am-2003-11-1224.
Koch-Müller, M., Dera, P., Fei, Y., Reno, B., Sobolev, N., Hauri, E., Wysoczanski, R., 2003. OH- in synthetic and natural coesite. Am. Mineral. 88, 1436–1445. https://doi.org/10.2138/am-2003-1007.
Koch-Müller, M., Abs-Wurmbach, I., Rhede, D., Kahlenberg, V., Matsyuk, S., 2007. Dehydration experiments on natural omphacites: qualitative and quantitative characterization by various spectroscopic methods. Phys. Chem. Miner. 34 (9), 663–678. https://doi.org/10.1007/s00269-007-0181-7.
Kurosawa, M., Yurimoto, H., Sueno, S., 1997. Patterns in the hydrogen and trace element compositions of mantle olivines. Phys. Chem. Miner. 24, 385–395. https://doi.org/10.1007/s002690050052.
Leahy, K., Taylor, W.R., 1997. The influence of the Glennie Domain deep structure on the diamonds in Saskatchewan kimberlites. Russ. Geol. Geophys. 38, 481–491.
Leost, I., Stachel, T., Brey, G.P., Harris, J.W., Ryabchikov, I.D., 2003. Diamond formation and source carbonation: mineral associations in diamonds from Namibia. Contrib. Mineral. Petrol. 145 (1), 15–24. https://doi.org/10.1007/s00410-003-0442-5.
Matsyuk, S.S., Langer, K., 2004. Hydroxyl in olivines from mantle xenoliths in kimberlites of the Siberian platform. Contrib. Mineral. Petrol. 147 (4), 413–437. https://doi.org/10.1007/s00410-003-0541-3.
Matsyuk, S.S., Langer, K., Hösch, A., 1998. Hydroxyl defects in garnets from mantle xenoliths in kimberlites of the Siberian platform. Contrib. Mineral. Petrol. 132, 163–179. https://doi.org/10.1007/s004100050414. Volume,.
Matveev, S., Stachel, T., 2009. Evaluation of kimberlite diamond potential using FTIR spectroscopy of xenocrystic olivine. Lithos 112, 36–40. https://doi.org/10.1016/j.lithos.2009.04.036.
Mikhail, S., Rinaldi, M., Mare, E.R., Sverjensky, D.A., 2021. A genetic metasomatic link between eclogitic and peridotitic diamond inclusions. Geochem. Perspect. Lett. 17, 33–38. https://doi.org/10.7185/geochemlet.2111.
Moine, B.N., Bolfan-Casanova, N., Radu, I.B., Ionov, D.A., Costin, G., Korsakov, A.V., Golovin, A.V., Oleinikov, O.B., Deloule, E., Cottin, J.Y., 2020. Molecular hydrogen in minerals as a clue to interpret ∂D variations in the mantle. Nat. Commun. 11 (1), 3604. https://doi.org/10.1038/s41467-020-17442-8.
Nestola, F., Jung, H., Taylor, L.A., 2017. Mineral inclusions in diamonds may be synchronous but not syngenetic. Nat. Commun. 8. https://doi.org/10.1038/ncomms14168.
Nimis, P., Alvaro, M., Nestola, F., Angel, R.J., Marquardt, K., Rustioni, G., Harris, J.W., Marone, F., 2016. First evidence of hydrous silicic fluid films around solid inclusions in gem-quality diamonds. Lithos 260, 384–389. https://doi.org/10.1016/j.lithos.2016.05.019. Elsevier B.V.
Novella, D., Frost, D.J., Hauri, E.H., Bureau, H., Raepsaet, C., Roberge, M., 2014. The distribution of H2O between silicate melt and nominally anhydrous peridotite and the onset of hydrous melting in the deep upper mantle. Earth Planet. Sci. Lett. 400, 1–13. https://doi.org/10.1016/j.epsl.2014.05.006.
Novella, D., Bolfan-Casanova, N., Nestola, F., Harris, J.W., 2015. H2O in olivine and garnet inclusions still trapped in diamonds from the Siberian craton: implications for the water content of cratonic lithosphere peridotites. Lithos 230, 180–183. https://doi.org/10.1016/j.lithos.2015.05.013.
Novella, D., Demouchy, S., Bolfan-Casanova, N., 2024. Deep hydrogen reservoirs and longevity. Elements 20 (4), 235–240. https://doi.org/10.2138/gselements.20.4.235.
O'Leary, J.A., Gaetani, G.A., Hauri, E.H., 2010. The effect of tetrahedral Al3+ on the partitioning of water between clinopyroxene and silicate melt. Earth Planet. Sci. Lett. 297 (1–2), 111–120. https://doi.org/10.1016/j.epsl.2010.06.011.
Palot, M., Jacobsen, S.D., Townsend, J.P., Nestola, F., Marquardt, K., Miyajima, N., Harris, J.W., Stachel, T., McCammon, C.A., Pearson, D.G., 2016. Evidence for H2O-bearing fluids in the lower mantle from diamond inclusion. Lithos 265, 237–243. https://doi.org/10.1016/j.lithos.2016.06.023.
Pearson, D.G., Brenker, F.E., Nestola, F., McNeill, J., Nasdala, L., Hutchison, M.T., Matveev, S., Mather, K., Silversmit, G., Schmitz, S., Vekemans, B., Vincze, L., 2014. Hydrous mantle transition zone indicated by ringwoodite included within diamond. Nature 507 (7491), 221–224. https://doi.org/10.1038/nature13080.
Peslier, A.H., Woodland, A.B., Bell, D.R., Lazarov, M., 2010. Olivine water contents in the continental lithosphere and the longevity of cratons. Nature 467 (7311), 78–81. https://doi.org/10.1038/nature09317.
Popovici, G., Wilson, R.G., Sung, T., Prelas, M.A., Khasawinah, S., 1995. Diffusion of boron, lithium, oxygen, hydrogen, and nitrogen in type IIa natural diamond. J. Appl. Phys. 77 (10), 5103–5106. https://doi.org/10.1063/1.359320.
Prencipe, M., Mantovani, L., Tribaudino, M., Bersani, D., Lottici, P.P., 2012. The Raman spectrum of diopside: a comparison between ab initio calculated and experimentally measured frequencies. Eur. J. Mineral. 24 (3), 457–464. https://doi.org/10.1127/0935-1221/2012/0024-2178.
Ragozin, A.L., Karimova, A.A., Litasov, K.D., Zedgenizov, D.A., Shatsky, V.S., 2014. Water content in minerals of mantle xenoliths from the Udachnaya pipe kimberlites (Yakutia). Russ. Geol. Geophys. 55 (4), 428–442. https://doi.org/10.1016/j.rgg.2014.03.002.
Skogby, H., 2006. In: Keppler, H., Smyth, J.R. (Eds.), Water in Natural Mantle Minerals I: Pyroxenes. Water in Nominally Anhydrous Minerals, pp. 155–167. https://doi.org/10.2138/rmg.2006.62.7. De Gruyter.
Skogby, H., Bell, D.R., Rossman, G.R., 1990. Hydroxide in pyroxene; variations in the natural environment. Am. Mineral. 75 (7–8), 764–774.
Smith, E.M., Krebs, M.Y., Genzel, P.-T., Brenker, F.E., 2022. Raman identification of inclusions in diamond. In: Smit, K., Shirey, S., Pearson, G., Stachel, T., Nestola, F., Moses, T. (Eds.), Diamond: Genesis, Mineralogy and Geochemistry. Mineralogical Society of America, pp. 451–473. https://doi.org/10.2138/rmg.2022.88.08. Issue 1.
Sokol, A.G., Kupriyanov, I.N., Palyanov, Y.N., 2013. Partitioning of H2O between olivine and carbonate-silicate melts at 6.3 GPa and 1400 °C: implications for kimberlite formation. Earth Planet. Sci. Lett. 383, 58–67. https://doi.org/10.1016/j.epsl.2013.09.030.
Stachel, T., Harris, J.W., 2008. The origin of cratonic diamonds - constraints from mineral inclusions. Ore Geol. Rev. 34 (1–2), 5–32. https://doi.org/10.1016/j.oregeorev.2007.05.002.
Stachel, T., Harris, J.W., 2009. Formation of diamond in the Earth's mantle. J. Phys. Condens. Matter 21 (36), 364206.
Taylor, L.A., Logvinova, A.M., Howarth, G.H., Liu, Y., Peslier, A.H., Rossman, G.R., Guan, Y., Chen, Y., Sobolev, N.V., 2016. Low water contents in diamond mineral inclusions: proto-genetic origin in a dry cratonic lithosphere. Earth Planet. Sci. Lett. 433, 125–132. https://doi.org/10.1016/j.epsl.2015.10.042.
Thomassot, E., Cartigny, P., Harris, J.W., Lorand, J.P., Rollion-Bard, C., Chaussidon, M., 2009. Metasomatic diamond growth: a multi-isotope study (13C, 15N, 33S, 34S) of sulphide inclusions and their host diamonds from Jwaneng (Botswana). Earth Planet. Sci. Lett. 282, 79–90. https://doi.org/10.1016/j.epsl.2009.03.001, 1–4.
Vangu, D., Bureau, H., Khodja, H., Charrondiere, M., Esteve, I., Béneut, K., Remusat, L., Gaillou, E., Cartigny, P., Bouillard, J.C., 2023. Combination of ERDA, FTIR spectroscopy and NanoSIMS for the characterization of hydrogen incorporation in natural diamonds. Diam. Relat. Mater. 136. https://doi.org/10.1016/j.diamond.2023.110007.
Weiss, Y., Czas, J., Navon, O., 2022. Fluid inclusions in fibrous diamonds. In: Smit, K., Shirey, S., Pearson, G., Stachel, T., Nestola, F., Moses, T. (Eds.), Diamond: Genesis, Mineralogy and Geochemistry. Mineralogical Society of America, pp. 475–532. https://doi.org/10.2138/rmg.2022.88.09.
Wiggers de Vries, D.F., Drury, M.R., de Winter, D.A.M., Bulanova, G.P., Pearson, D.G., Davies, G.R., 2011. Three-dimensional cathodoluminescence imaging and electron backscatter diffraction: tools for studying the genetic nature of diamond inclusions. Contrib. Mineral. Petrol. 161 (4), 565–579. https://doi.org/10.1007/s00410-010-0550-y.
Withers, A.C., Bureau, H., Raepsaet, C., Hirschmann, M.M., 2012. Calibration of infrared spectroscopy by elastic recoil detection analysis of H in synthetic olivine. Chem. Geol. 334, 92–98. https://doi.org/10.1016/j.chemgeo.2012.10.002.
Yang, X., Liu, D., Xia, Q., 2014. CO2-induced small water solubility in olivine and implications for properties of the shallow mantle. Earth Planet. Sci. Lett. 403, 37–47. https://doi.org/10.1016/j.epsl.2014.06.025.